Atmospheric Environment Vol. 27A, No. 17/18, pp. 2895–2899, 1993.
Printed in Great Britain.

0004-6981/93 $6.00+0.00
Pergamon Press Ltd

OPTICAL DEPTHS AND HAZE PARTICLE SIZES DURING AGASP III

PETER PILEWSKIE and FRANCISCO P. J. VALERO

NASA Ames Research Center, Atmospheric Physics Research Branch, M/S 245-4, Moffett Field, CA 94035-1000, U.S.A.

(*First received* 14 *February* 1992 *and in final form* 24 *June* 1993)

Abstract—The optical properties of Arctic Haze were studied using a total–direct–diffuse radiometer as part of the Arctic Gas and Aerosol Sampling Project, part III (AGASP III). The radiometer was installed on the NOAA WP-3D research aircraft and measured solar downwelling irradiance in seven narrow-band channels in the visible and near-infra-red. Haze optical depths had maximum values near 0.1 in the mid-visible for AGASP flights 310 and 311. An inferred particle size spectrum from flight 311 extinction measurements showed two dominant modes near 0.1 and 0.8 μm. A method of retrieving the angular dependence of scattered radiation is presented and suggests the presence of thin cirrus.

Key word index: Aerosols, optical depth, particle size spectrum, Arctic Haze.

1. INTRODUCTION

Interactions between solar and infra-red radiation and the polluted Arctic atmosphere are climatically important. Arctic aerosols interact with solar radiation mostly in late winter and early spring, when aerosol concentration is at or near maximum and the sun is high enough for significant solar radiation to reach the Arctic. Since ice at the polar regions reflects about 80% of the incident solar energy, much of that radiation passes twice through the haze layers, resulting in increased absorption. As more energy is retained by the aerosol, atmospheric warming is enhanced. Increased atmospheric scattering and absorption result in less solar energy reaching the ground, and the changed energy absorption profile in the atmosphere further modifies the energetics of the atmosphere–surface system.

To gain insight into these processes we must know the physical and radiative properties of the aerosols: particle composition, size, cloud thickness, and aerosol absorption and scattering parameters. Shaw (1982), Bodhaine *et al.* (1984), and Dutton *et al.* (1984) have reported surface-based measurements of optical depth in the Arctic; Valero *et al.* (1983, 1984, 1989) measured haze absorption *in situ*; Rosen and Novakov (1981) and Rosen and Hansen (1984) reported that graphitic carbon (soot) is the component responsible for most of the solar energy absorption.

Initial steps towards increasing our understanding of the effects of Arctic Haze have been undertaken in the Arctic Gas and Aerosol Sampling Project. This paper presents some of the optical measurements of the Arctic Haze from the third AGASP experiment in March of 1989. Encounters with haze layers during special radiation flight legs were infrequent during AGASP III. We present data from two flights when haze extinction was found to be significant. Typically, surface or aircraft measurements usually comprise the atmospheric columnar extinction above the observation site, leading to ambiguous interpretations on the effects of the haze unless reasonable assumptions on the background stratospheric and background tropospheric aerosol extinction are made. Our approach, however, has been to isolate individual layers. The values of columnar extinction presented in this paper can be attributed almost entirely to haze.

2. EXPERIMENTAL

During the Arctic Gas and Aerosol Sampling Project third field experiment (AGASP III) in March 1989, the NASA Ames Atmospheric Physics Research Branch deployed a Total–Direct–Diffuse Radiometer (TDDR) to study Arctic Haze optical properties. Mounted atop the fuselage of the NOAA WP-3D research aircraft, the TDDR measured the downwelling hemispherical irradiance in seven narrow-band spectral regions: 380, 412, 500, 675, 776, 862 and 1064 nm. Band-centers were chosen to minimize the influence of gaseous absorption, thereby isolating the optical effects of aerosols.

Direct solar irradiance was acquired through the use of an oscillating shadow arm that occluded the solar disk, rendering only scattered light. By subtracting this amount from the total irradiance, i.e. the signal measured when the shadow arm was entirely out of the hemispherical field, direct solar irradiance was obtained. A correction for the diffuse radiation blocked by the shadow arm (including forward scattered light) was made by interpolating through the arm shadow.

An example of raw TDDR data is shown in Fig. 1. A sharp discontinuity in the slope of the data occurs as the arm shadow begins to sweep across the diffuser. The raw signal at this discontinuity represents the total flux minus an amount scattered in the near-forward direction. The points indicated by "Sun blocked" in Fig. 1 represent the total flux minus the direct solar flux minus a forward scattered flux similar, but not necessarily equal, in magnitude to the amount at the

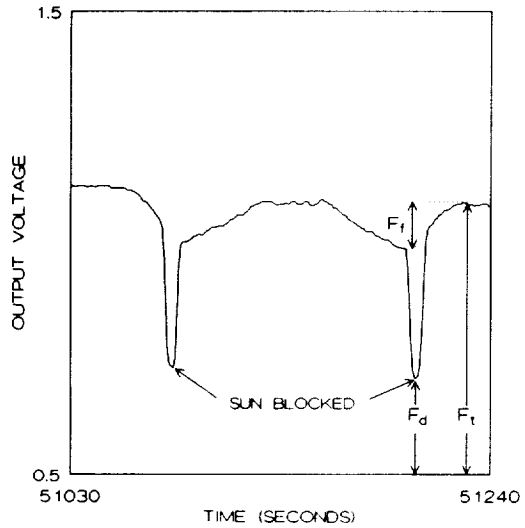

Fig. 1. Sample of raw TDDR data. F_t indicates the total flux, F_d the diffuse flux unshielded by the shadow arm, and F_f the diffuse flux shielded by the shadow arm.

discontinuity. We account for that difference by interpolating across the spike. A complete instrument model which simulates TDDR measurements is briefly described in the last section. Using this model, it has been found that the interpolation method is adequate to account for the forward scattering correction.

From the TDDR-measured solar irradiances we determined aerosol optical depth, τ_a, from the Beer–Lambert law of extinction

$$\tau_a = \ln(F_1/F_2)/m - \tau_r.$$

Here τ_r is the Rayleigh optical thickness, determined by the pressure difference between layers 1 and 2; F_1 and F_2 are the direct solar flux at those levels, in arbitrary units; m is the relative airmass, or the ratio of the slantpath to the zenith path. An empirical expression to account for the curvature of the atmosphere has been given by Rozenberg (1966)

$$m = \{\cos\theta + 0.025\exp(-11\cos\theta)\}^{-1}$$

where θ is the solar zenith angle. For $\theta < 80^\circ$, $m \simeq$ secant θ. The results presented in this paper are derived from measurements made with $\theta < 80^\circ$.

Determining aerosol extinction in the manner just described affords several advantages that increase the accuracy of the derived optical thickness. Since only relative measurements are necessary, independent field or laboratory

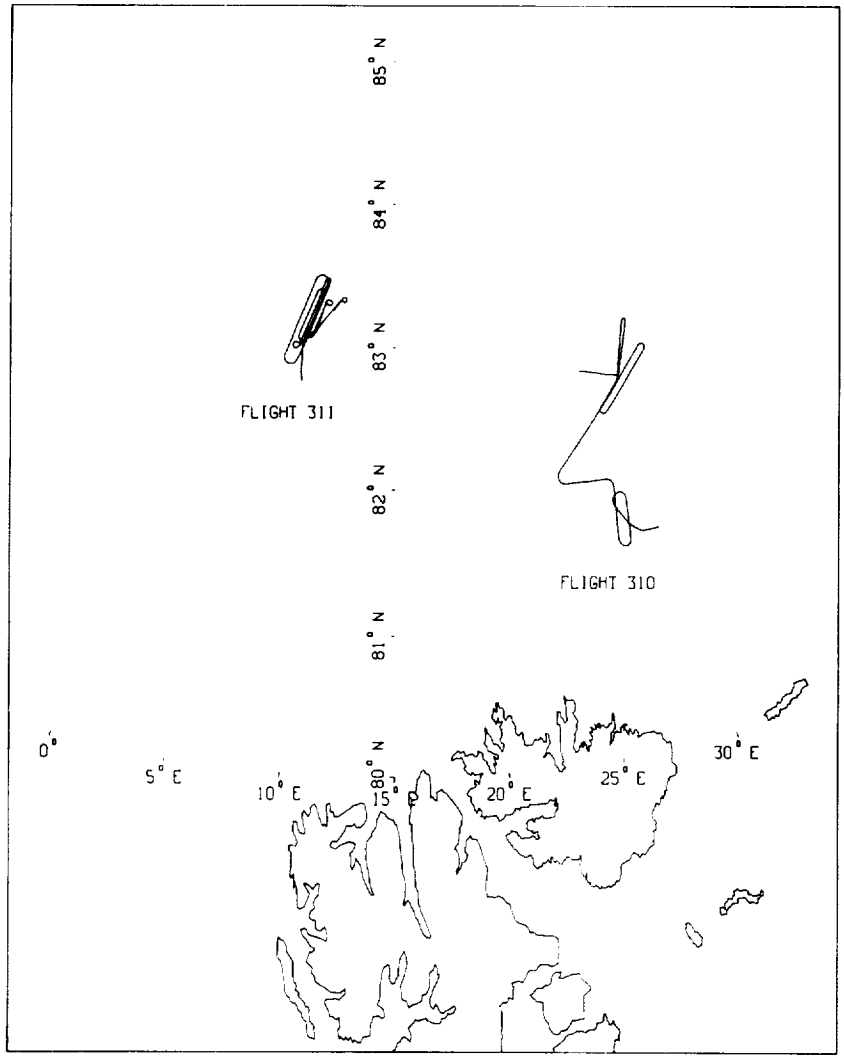

Fig. 2. Radiation leg segments of flight tracks 310 and 311.

calibrations with their associated errors become obsolete. Furthermore, NO_2 and O_3 absorption, which may have a small influence on the four short-wavelength channels, is removed by subtraction. Even Rayleigh optical thickness, which can be computed quite accurately from the pressure, is nearly entirely removed by isolating the shallow haze layers. Errors for the optical thickness reported in this research were determined to be less than 10%.

3. OPTICAL DEPTHS AND PARTICLE SIZES

We present here data acquired during AGASP flights 310 and 311 on 29 and 31 March, respectively. Both flights 310 and 311 included radiation legs with tracks specially designed to accommodate the measurement of haze optical thickness. These legs consisted of a series of stacked loops above and beneath significant haze layers and aligned with the solar azimuth. Each loop then comprised legs of approximately 5 min duration toward and away from the sun. The radiation tracks for flights 310 and 311 are shown in Fig. 2. The flight 310 radiation leg isolated one haze layer between 100 and 7700 m, over ice, in the vicinity of 30°E, 82°N; for flight 311, three layers were isolated, with the top at 6400 m, bottom at 200 m, and intermediate levels at 500 and 2000 m, also over ice, near 10°E, 83°N.

Rather than attempt to describe the spatial and temporal variability of haze layers, we sought to define each layer by averages over the flight tracks. Having two nearly identical tracks but in opposing directions at every level proved beneficial in correcting for TDDR zenith dependence, which becomes significant at the low solar elevation in the arctic. Average radiative flux values were determined for each flight level and the direct solar fluxes were extracted; finally, the optical thickness of the intervening layer was calculated from the Beer–Lambert law.

Haze optical depths for the AGASP flights 310 and 311 between the levels indicated previously are shown in Fig. 3. The data presented here has been corrected for platform orientation and forward scattered radiation in the field of the TDDR shadow arm. For contrast, also shown in Fig. 3, are optical depths from flight 201, during AGASP II in 1986. The optical depths of the haze layers encountered on flights 310 and 311 were near the average for the Alaskan arctic spring, around 0.1, reported by Shaw (1982) and Dutton *et al.* (1984); those from the previous mission, flight 201, were similar in magnitude to the maximum surface-derived estimates (Shaw, 1982).

The spectral optical depths from flight 311 were used to derive a haze particle size distribution following a procedure outlined by King *et al.* (1978). The resulting columnar size distribution is displayed in Fig. 4. The distribution is bimodal with an accumulation mode near 0.1 μm and a large particle mode near 0.8 μm. The sensitivity of the inversion to the limits on distribution radii are well documented (King *et al.*, 1978). As such, Fig. 4 should be interpreted somewhat loosely. Radius limits here were chosen for stability and to best reproduce the measured extinction: model and measurements agreed to within 10% at all wavelengths. The significant conclusion is that the size

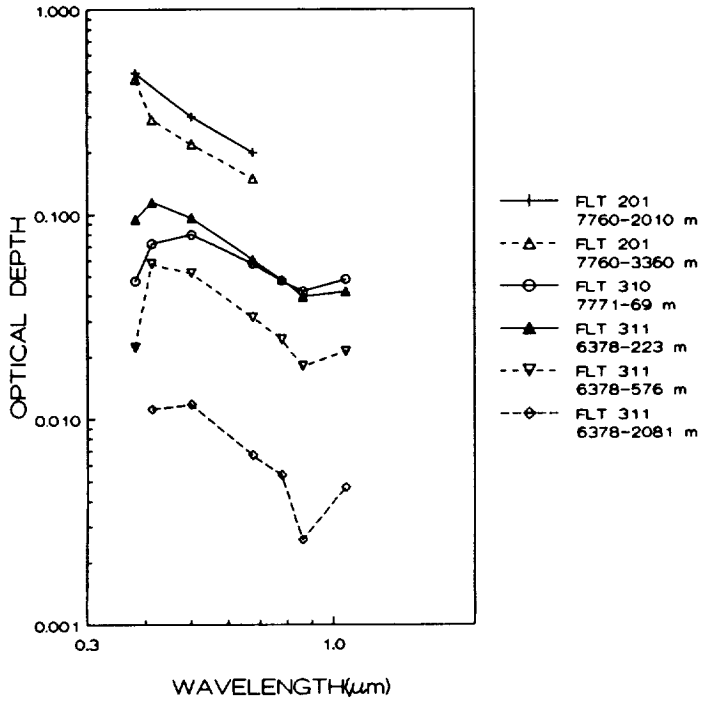

Fig. 3. AGASP flights 310 and 311 optical depths in several layers. Flight 201 data is shown for comparison.

distribution that results in the extinction spectra shown in Fig. 3 is most likely bimodal.

The minimum extinction at 862 nm was found in all spectra on both flights 310 and 311. Later calibration of the TDDR indicated this effect was not instrumental. Such a local extinction minimum is a strong indicator of an optically dominant size mode. For a minimum at 862 nm, simple diffraction theory (see for example, Bohren and Huffman, 1983) would suggest a particle size of around 0.85 μm (for a real refractive index of 1.5).

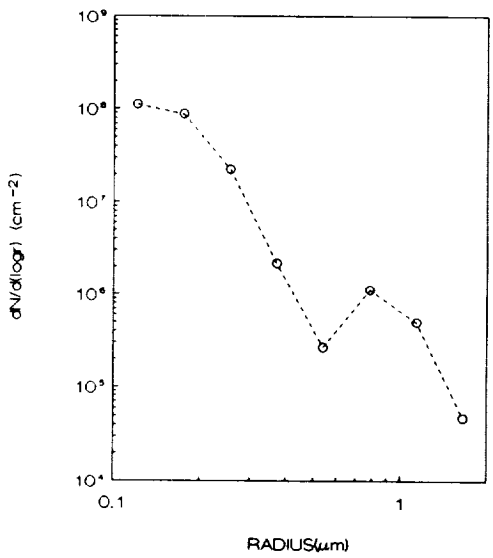

Fig. 4. Columnar size distribution from flight 311 data.

4. THE ANGULAR DEPENDENT RADIATION FIELD

As illustrated in the sample of raw data shown in Fig. 1, the effect of the TDDR shadow arm is apparent well before and after the direct beam is occluded. For optically thick layers, the influence off the shadow arm on the diffuse flux is striking. Reduction in diffuse radiation is greatest when the shadow arm is directly overhead (90° elevation), regardless of solar position, due to the cosine weighting of downwelling irradiance.

When such a response in the diffuse flux occurs, it seems plausible to retrieve the angularly dependent diffuse radiance field, or some effective weighted average. Since the shadow arm is in continuous motion and we sample throughout the rotation cycle, we measure hemispherical flux minus a great circle belt of radiation that is dependent upon shadow arm position. Information from successive measurements retains some independence since the "blacked out" belts change with the motion of the shadow arm.

The quantity measured by the TDDR is a radiative flux defined by

$$F=\int_{\lambda}\int_{\Omega}\int_{a} I_{\lambda}(\mu,\varphi)R(\lambda)\cos\psi\ \mathrm{d}a\ \mathrm{d}\Omega\,\mathrm{d}\lambda$$

where I_λ is the monochromatic intensity in the wavelength interval λ, $\lambda+\mathrm{d}\lambda$, ψ is the angle an incoming ray makes with the normal to the detector element, Ω is the detector solid angle, μ is the cosine of the zenith, φ is the azimuth, $R(\lambda)$ is the detector response function, and a is the detector area. If we assume that the system response is flat over the interference filter half-band width (10 nm) and incident radiance does not vary significantly over the surface of the detector we can immediately integrate over area and wavelength so that

$$F\alpha\int_{\Omega} I_{\lambda}(\mu,\varphi)\cos\psi\ \mathrm{d}\Omega.$$

Retrieval of I_λ (or some representative average) from the total–direct–diffuse measurements is conceivable because the collection of downward-directed rays that contributes to the measured flux are determined in part by the shadow-arm position. Although the solid angle subtended by the shadow arm is independent of shadow-arm position, the cosine weighting of the blacked-out belts is not. Measurements resulting from n different shadow-arm positions can be written

$$F_1=\int_{\Omega_1} I_{\lambda}(\mu,\varphi)\cos\psi\ \mathrm{d}\Omega$$

$$F_2=\int_{\Omega_2} I_{\lambda}(\mu,\varphi)\cos\psi\ \mathrm{d}\Omega$$

$$\vdots$$

$$F_n=\int_{\Omega_n} I_{\lambda}(\mu,\varphi)\cos\psi\ \mathrm{d}\Omega.$$

A final step before solving this system of equations is to consider the average intensity over belts parallel to the shadow arm, thus reducing the problem to a single dimension. A series of linear equations result, and have the discrete form:

$$F=\sum_i w_i\bar{I}_i$$

where $\bar{I}_i$ is now the average intensity over the ith belt; the weighting vector w is a function of shadow-arm position.

We chose to solve the system of equations using the Twomey–Chahine iterative, nonlinear method which lends itself well to large systems of equations. (See Twomey *et al.*, 1977.) We solved for the longitudinally averaged radiances using data acquired from flight 311 when the aircraft was at an altitude of 800 m. This data was not acquired during a dedicated radiation leg such as that reported in Section 3, and the concurrent optical thickness is not available.

The results are shown in Fig. 5, where normalized average intensity is plotted vs scattering angle from

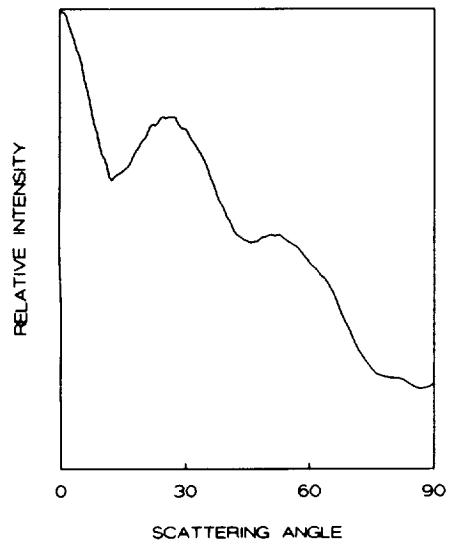

Fig. 5. Normalized intensity averaged over belts parallel to TDDR shadow arm. The scattering angle is measured in degrees from the Sun.

the Sun. It should be noted that solar position was correctly matched by the forward scattering peaks. The results shown here represent the first step towards deriving particle phases function; the TDDR is being modified to accommodate the retrieval of intensity as a function of two independent angular variables. However, one inference may be made from the results shown in Fig. 5: the secondary and tertiary maxima occur close to the halo angles for hexagonal ice crystals (22 and 48° for blue light), suggesting the possible presence of very thin (perhaps invisible) cirrus. The flight log at that time makes no note of the presence of cirrus.

5. CONCLUSIONS

We have presented measured spectral optical depths from AGASP flights 310 and 311. Peak visible optical depths were near 0.1 for both flights, similar in magnitude to surface derived haze optical depths over Alaska. Since the measurements isolated individual haze layers, no corrections for background extinction were necessary. Inferred size spectra show peak concentrations in the accumulation mode at 0.1 μm and a secondary peak near 0.8 μm. Analysis of the angular-dependent scattered radiation field from a different flight segment suggests the presence of a thin cirrus.

Acknowledgements—Warren Gore, Larry Pezzolo, and Melinda Weil supported this effort both in the field and in the preparation of instrumentation.

REFERENCES

Bodhaine B. A., Dutton E. G. and DeLuisi J. J. (1984) Surface aerosol measurements at Barrow during AGASP. *Geophys. Res. Lett.* **11**, 377–380.

Bohren C. F. and Huffman D. R. (1983) *Absorption and Scattering of Light by Small Particles.* John Wiley & Sons, New York.

Dutton E. G., Deluisi J. J. and Bodhaine B. A. (1984) Features of aerosol optical depth observed at Barrow, March 10–20, 1983. *Geophys. Res. Lett.* **11**, 385–388.

King M. D., Byrne D. M., Herman B. M. and Reagan J. A. (1978) Aerosol size distributions obtained by inversion of spectral optical depth measurements. *J. atmos. Sci.* **35**, 2153–2167.

Rosen H. and Novakov T. (1981) Combustion-generated carbon particles in the arctic atmosphere. *Nature* **306**, 768–780.

Rosen H. and Hansen A. D. A. (1984) Role of combustion-generated carbon particles in the absorption of solar radiation in the arctic haze. *Geophys. Res. Lett.* **11**, 461–464.

Rozenberg G. V. (1966) *Twilight: a Study in Atmospheric Optics.* Plenum Press [translated from the Russian], New York.

Shaw G. E. (1982) Atmospheric turbidity in the polar regions. *J. appl. Met.* **21**, 1080–1088.

Twomey S., Herman B. and Rabinoff R. (1977) An extension to the Chahine method of inverting the radiative transfer equation. *J. atmos. Sci.* **34**, 1085–1090.

Valero F. P. J. (1984) The absorption of solar radiation by the arctic atmosphere during the haze season and its effects on the radiation budget. *Geophys. Res. Lett.* **11**, 465–468.

Valero F. P. J., Ackerman T. P. and Gore W. J. Y. (1983) Radiative effects of the arctic haze. *Geophys. Res. Lett.* **10**, 1184–1187.

Valero F. P. J., Ackerman T. P. and Gore W. J. Y. (1989) The effects of the arctic haze as determined from airborne radiometric measurements during AGASP II. *J. atmos. Chem.* **9**, 225–244.